# Degradation of the CaF$_2$(111) surface by air exposure

M. Reichling *, M. Huisinga, S. Gogoll, C. Barth

*Fachbereich Physik, Freie Universität Berlin, Arnimallee 14, 14195 Berlin, Germany*

## Abstract

We investigate the electronic and geometric structure of CaF$_2$(111) surfaces produced by cleavage in air in comparison to surfaces cleaved in an ultra-high vacuum. An analysis with ultraviolet photoelectron spectroscopy reveals a broadening of the fluorine 2p valence band peak, the formation of a broad band of occupied electronic states extending into the band gap and an increase in electron scattering after the surface has been exposed to air. We attribute these effects to the incorporation of gas molecules into the crystal and chemical reactions at the surface. Surface modifications appear as stable, nanometer-sized patches of reactants that can be directly observed by scanning force microscopy. These patches are found to be randomly distributed over the surface and have a height never exceeding the minimum possible step height on the CaF$_2$(111) surface. Furthermore, it is demonstrated that oxygen in the crystal can be transformed into CaO when metallising the surface and near surface bulk by low-energy electron irradiation. Oxidation is strongly enhanced by electron-stimulated diffusion of oxygen. By monitoring oxidation in a shallow surface layer with X-ray photoelectron spectroscopy, we also monitor thermally activated diffusion of oxygen to the surface after electron irradiation. © 1999 Elsevier Science B.V. All rights reserved.

## 1. Introduction

In recent years, calcium difluoride has gained great importance as an optical material in the ultraviolet spectral range. Providing high transmission for light of a wavelength down to 130 nm [1], it is one of the very few materials suitable for optics operated in the deep ultraviolet spectral range, especially for the next generation laser lithography machines operating at a wavelength of 193 nm (Ref. [2] provides a compilation of several articles about topics related to laser lithography at 193 nm).

A severe limitation in the development of equipment for ultraviolet laser lithography, however, is the degradation and destruction of optical components by a large number of intense laser pulses [3]. It is known that for 248 nm light, the detrimental interaction of laser light with highest purity materials is exclusively determined by surface properties [4], and the resistivity against damage and ablation may be increased by a factor of more than two by advanced surface preparation techniques [4,5]. Advancements in grinding and polishing techniques for brittle optical surfaces yield both a reduction in light absorbing surface defects and

---

* Corresponding author. Fax: +49-30-838-6059.
*E-mail address:* reichling@physik.fu-berlin.de (M. Reichling)

structural imperfections causing mechanical instability [6]. The ultimate limit of damage resistivity, however, is defined by the properties of the most 'perfect' surface that can be produced and used in a standard industrial environment, i.e. the properties of flat terraces on a crystal, cleaved and handled in air.

In an effort to explore this limit, the present paper is devoted to the characterisation of crystals cleaved in air along the (111) natural cleavage plane with respect to their surface geometric and electronic structure in comparison to properties of surfaces produced by cleavage in an ultra-high vacuum. We demonstrate that air cleavage results in chemical reactions of components of the ambient air with the surface introducing a small but significant roughness in the form of nanometer-sized patches of reactants covering the surface in a random pattern. Correspondingly the electronic structure exhibits a broad band of occupied states extending into the band gap. We demonstrate furthermore that oxygen plays a major role in the surface degradation process and that the original surface reactants may be transformed into CaO by irradiation of the surface with low-energy (2.5 keV) electrons. The process is explained in terms of a model involving diffusion and activation enhanced by the electron impact. For our investigations, we used three different experimental techniques, namely ultraviolet photoelectron spectroscopy (UPS) to sensitively detect band-gap states and effects of oxygen uptake in a surface layer, X-ray photoelectron spectroscopy (XPS) with a lower sampling depth[1] to monitor surface oxidation and its creation by diffusion of oxygen from the bulk to the surface and scanning force microscopy (SFM) to reveal the geometric structure of clean and air-exposed surfaces.

---

[1] The sampling depth for 1 keV photoelectrons emitted in our XPS measurements can be determined from the universal curve for the mean free path of electrons in matter (e.g. see Ref. [11], p. 7). The universal curve does not apply to photoelectrons with kinetic energies below the inelastic electron–electron scattering limit that are relevant for our UPS studies. We determined a UPS sampling depth of several nanometers in photoemission experiments on $CaF_2$ epitaxial thin films of various thickness. Detailed results will be published elsewhere.

## 2. Experimental

Samples were commercial high-purity (111)-oriented $CaF_2$ crystals either cleaved in air and then transferred into an ultra-high vacuum (UHV) environment or cleaved in situ. Rectangular ($20 \times 20 \times 3$ mm$^3$) or rod-like (6 mm diameter) crystals were mounted in a titanium sample holder that could be heated by means of resistive heater elements. To remove surface contaminants, crystals were heated up to 700 K for 30 min prior to measurements. The base pressure in our UHV systems was below $5 \times 10^{-8}$ Pa. During heating, the pressure attained higher values but never exceeded a level of $10^{-7}$ Pa for more than a few minutes. UPS was performed with unpolarised light from an ultraviolet (UV) discharge source operated at 21.2 eV (He I line). Except for one series of measurements, photoelectrons were recorded in normal emission by a hemispherical double-pass analyser providing 100 meV energy resolution. In all UPS results displayed below, the electron yield is plotted as a function of the electron kinetic energy as determined with the analyser since a conversion to binding energies is difficult in some cases due to charging effects and is not necessary for our purposes. XPS measurements were made under similar conditions in a separate vacuum system with 1487 eV photons (AlK$_\alpha$ line). In this case, the electron energy analysis was accomplished by a single-pass hemispherical analyser, and an overall energy resolution of 1 eV was obtained. The binding energies given for the X-ray photoelectron spectra presented below have been derived from the measured kinetic energies by relating them to the Fermi level of the analyser. To stimulate surface oxidation, in some experiments, the surface was irradiated with 2.5 keV electrons from a source providing a defocused beam with an almost homogeneous intensity variable from 50 to 200 μA/cm$^2$ at the sample surface. The surface area from which photoelectrons were sampled in both cases was much smaller than the square of $4 \times 4$ mm$^2$ irradiated with electrons. The sample temperature during electron irradiation was kept constant in all experiments at a value of about 400 K. SFM micrographs were taken at room temperature with a commercial

UHV scanning force microscope operated in the dynamic mode, as described in detail elsewhere [7].

There are two important issues arising from the surface analysis on dielectric crystals, both related to the poor conductivity of this class of materials: first, is the experimental result influenced by sample charging, and, second, to what extent is the surface modified by the process of measurements? In the case of SFM measurements, we tested the resolution and calibration at step edges and took care to avoid artefacts due to local charges by heating samples prior to the measurements. We can exclude any scanning-induced surface alteration since the interaction of the SFM tip with the surface is very weak in the dynamic mode of operation. This, however, is not as straightforward for a photoemission experiment. Bulk insulating crystals have a tendency to charge up during photon irradiation where the charge may result in a shift, broadening or even suppression of photoemission features in the spectra. In a previous study [8], we investigated such effects in detail and presented methods of how to reduce or fully compensate charging. In some measurements presented here, we found charging in the form of a slight shift of photoemission spectra on the kinetic energy scale. However, since the interpretation of our results does not depend on the absolute position of photoemission features, none of the conclusions presented here is affected by charging in any way.

A much more severe problem related to our photoemission studies is sample damage. Both photons from our UPS and the XPS source are known to create permanent damage in a $CaF_2$ crystal mostly in the form of F center defects [9]. The impact of the low-energy photons used for UPS on an air-cleaved sample is demonstrated in Fig. 1. The main features in such a spectrum are the F 2p peak, and a much weaker emission in the band-gap region that will be discussed in detail in Section 3. Here, we note that the band-gap emission is reduced by a certain factor due to irradiation for 225 min, whereas we observe a strong increase in secondary electron emission with very low kinetic energies. The important result is, however, that the relative loss of intensity in the band-gap region is the same for all energies, and no new spectral features appear upon prolonged irradia-
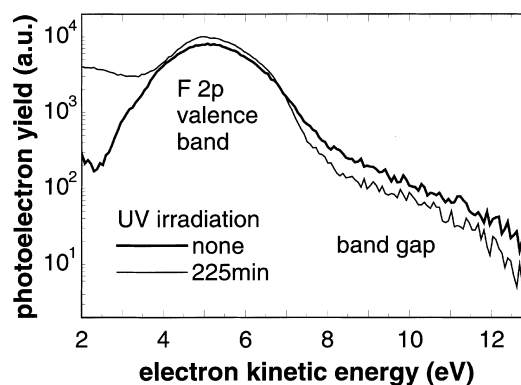


Fig. 1. Demonstration of the influence of continued irradiation with 21.2 eV photons on the ultraviolet photoemission spectrum of $CaF_2(111)$. The logarithm of the normal emission photoelectron yield at the beginning and 225 min after the start of the irradiation is plotted as a function of electron kinetic energy.

tion. Corresponding results have been obtained for XPS measurements, where we found clear evidence of F center production upon prolonged irradiation in earlier experiments [10]. In both cases, defect production is below a level that would affect our observations. As will be shown below, however, electron irradiation as applied here has a tremendous effect on both UPS and XPS spectra of air-cleaved crystals. This can be understood by considering that this type of irradiation provides an energy input density and, hence, defect creation density that is at least three orders of magnitude larger than that of the photons[2]. In various experiments we found that the concentration of air exposure related impurities is much smaller than the electron irradiation induced defect density.

## 3. Structure of air- and UHV-cleaved surfaces

A major goal of the present work is the investigation of the influence of air exposure on surfaces prepared by cleavage. To accomplish this, we

---

[2] The energy deposition density for electrons is 270 eV/$nm^3$s assuming a beam of 2.5 keV electrons with an intensity of 50 μA/$cm^2$ and a penetration depth of 30 nm. For the 21.2 eV photons of our UPS source, we find a deposition density of 0.19 eV/$nm^3$s, assuming a flux of $2 \times 10^{11}$/s photons distributed over a spot of 1.5 mm diameter penetrating 13 nm into the sample.

performed direct comparisons, i.e. cleaved crystals under identical conditions and applied exactly the same surface treatment except that cleavage of one of the crystals was performed in UHV, whereas the other was cleaved in ambient air. For a comparison of the electronic structures, we applied UPS probing occupied states in the valence band and the band gap. A typical spectrum probing emission normal to the sample surface is shown in Fig. 2 in a logarithmic representation of data to better visualise the small electron yield in the band-gap region. There are three features distinguishing the spectrum of the air-cleaved sample from that of the surface prepared by UHV cleavage. First, the emission in the band-gap region is much stronger and tails further into the band gap. Second, the valence band peak (F 2p) is somewhat broadened, and, third, the secondary electron emission is strongly enhanced. By cleaving samples in UHV and then exposing them to air prior to UPS investigation, we confirmed that the appearance of all features is caused by exposure to air and does not require air to be present during the process of cleavage.

The first observation is clear proof that air cleavage introduces a large number of additional band-gap states and that these states are not due to cleavage-related structural imperfections but are impurity states created by air exposure of the surface. The intensity of the band gap emission

from different air-cleaved samples varied between measurements, but in all cases, the emission was much stronger than for UHV-cleaved samples. The band gap emission tail for the air-cleaved samples extends to energies up to 9.5 eV above the normal emission peak of the valence band. At present, the nature of valence band broadening and its relation to band-gap states is not yet clear, but we assume that it is a result of oxygen dissolved in the crystal lattice and thus closely related to the process of stimulated oxidation discussed below.

The other features apparent in Fig. 2 are attributed to the introduction of surface roughness or defects created by air exposure within the UPS sampling depth. It is well known that such imperfections cause scattering of photoelectrons when introduced into a perfect crystal [11]. Such scattering results in a reduction in photoemission intensity in the region of higher kinetic energies and causes a high yield of secondary electrons with a very low kinetic energy, as is evident from the comparison of spectra shown in Fig. 2. Even stronger evidence for the presence of electron scattering is found in photoelectron spectra with angular resolution, as presented in Fig. 3. The upper traces show spectra from a UHV-cleaved crystal with two peaks varying in relative intensities upon changing the angle of emission, which is very similar to our observations when growing epitaxial $CaF_2$ thin films and would be expected for a perfectly crystalline surface [12]. The total valence band emission intensity, however, does not change dramatically when sampling in different directions. The picture is completely different for a measurement on the air-cleaved sample shown in the lower frame. There, the angle-dependent valence band structure is completely smeared out, and the valence band emission intensity strongly decreases when photoelectrons pass a thicker sheet of material for observation under a small angle with the surface. However, the yield of secondary electrons is strongly enhanced for all emission angles when compared to the spectra obtained from the UHV-cleaved crystal.

The UPS results suggest a significant structural modification when exposing the surface to air. To verify this modification on a nanoscopic scale, we applied scanning force microscopy and imaged
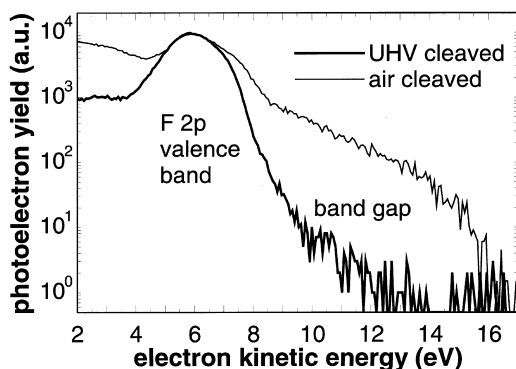


Fig. 2. Comparison of ultraviolet photoemission spectra of surfaces prepared by cleavage in UHV and air. The logarithm of the normal emission photoelectron yield is plotted as a function of electron kinetic energy. Yield curves have been scaled and shifted in energy so that the maxima of both curves coincide.
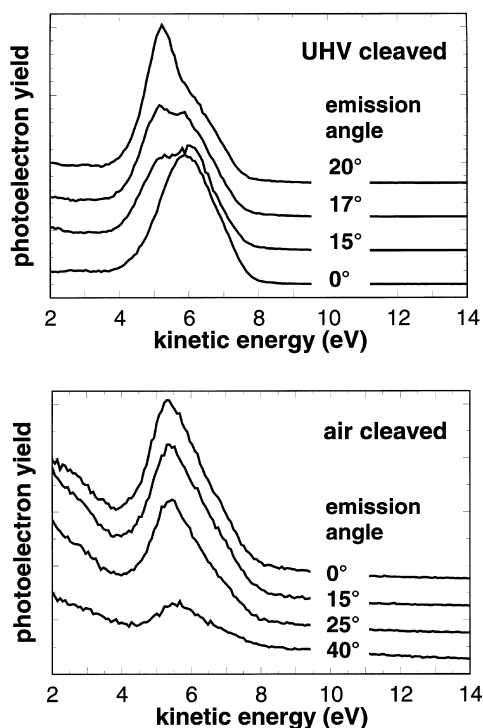
Fig. 3. Comparison of angle-resolved ultraviolet photoemission spectra of surfaces prepared by cleavage in UHV and air.
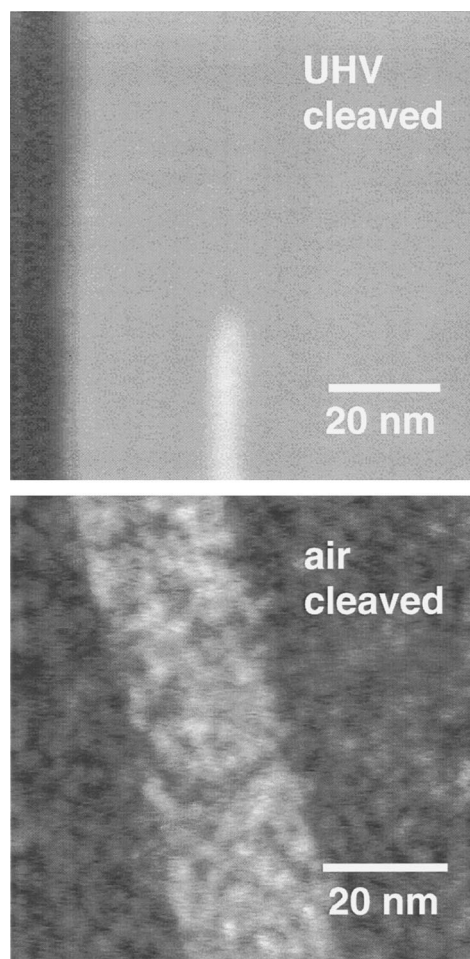


Fig. 4. Comparison of scanning force micrographs obtained on surfaces prepared by cleavage in UHV and air. The apparent steps have a height of 0.32 nm corresponding to the height of a F–Ca–F triple layer on the $CaF_2(111)$ surface.

equivalent surface regions of UHV and air-cleaved crystals. Typical examples are shown in Fig. 4. In the upper micrograph showing the result for the UHV cleavage, we find an atomically flat terrace and steps with a height of 0.32 nm corresponding to the height of a F–Ca–F triple layer of the fluorite structure. As the surface was imaged a short time after cleavage, we did not detect any signs of contamination. A completely different topography is found for the air-cleaved surface exhibiting a strong corrugation in the form of a granular structure. Terraces and edges are covered with nanometer-sized patches that are randomly distributed over the surface. These structures turned out to be absolutely stable during repetitive scanning also with a higher resolution and were found to have lateral dimensions of a few nanometers. Presently, it is not possible to image such features with a resolution higher than several nanometers or to reveal the internal structure of the patches. However, we note several common fea-

tures in a series of measurements on different areas of the sample and comparative studies on different samples. First, it is found that even as the dosage of various gases is extremely high during air exposure, the surface is never completely covered with patches, but we always find surface regions where the flat $CaF_2$ surface is present. Therefore, we conclude that the progression of surface degradation is limited by some property of the surface or limiting process rather than by the supply of reactants. Second, we find patches with a significant variation in lateral size and elevation, but

their height is always smaller than the triple-layer step height. This is clear-cut proof that the observed features are not composed of $CaF_2$ or are the result of surface metallisation [13]. Third, it is found that the surface structure is rather stable against thermal treatment. In a series of measurements, our force microscope does not allow imaging of the same area during or shortly after heating; however, when imaging the surface in different areas before and after heating to a temperature of 440 K for several hours we cannot recognise significant differences in surface topography. This suggests that the patches formed at the surface are the product of chemical reactions rather than a physisorption of gases.

So far, we have shown that air exposure of $CaF_2(111)$ results in dramatic changes to the surface structure on a nanometer scale induced by reactions between constituents of the air and the surface, but neither UPS nor scanning force imaging yields any information about the chemical structure of the modified surface. Whereas the latter is not sensitive to the chemical composition, photoelectron spectra in the band-gap region are rather unspecific, and certain constituents cannot be identified. In Section 4, we will demonstrate that oxygen plays a major role in the surface degradation process and that, in fact, not only is oxygen involved in surface chemistry, but upon air exposure, it also penetrates into the depth of the material.

## 4. Electron-stimulated oxidation

The experimental strategy to reveal the role of oxygen in the degradation process is based on irradiation of the surface with low-energy electrons, metallising the surface and a near-surface layer. Metallic clusters formed by this process are oxidised by oxygen dissolved in the crystal, and thus, the oxygen is transformed into a specific chemical state that can be identified by UPS and XPS. We find that electron irradiation not only activates oxide formation but also stimulates the diffusive transport of oxygen from the bulk to the surface. The basic experiments along these lines have already been introduced in previous work

[14], and these studies are continued here in a more systematic way. In Ref. [14], we have shown that electron irradiation of a UHV-cleaved crystal does not result in any specific change in band-gap photoemission, as measured by UPS while we observed the development of a band-gap feature when irradiating an air-cleaved crystal.

Here, we prepared several spots on an air-cleaved crystal by irradiation with various electron dosage densities up to 1 C/cm². The dosage density was varied by irradiating for different times at different current density levels ranging from 60 to 180 μA/cm². Electron irradiation was performed at a sample temperature of 400 K, and UPS measurements were performed after heating the crystal to 490 K to reduce charging. It was found that the critical parameter to obtain a specific oxidation result is the dosage density independent of the apparent current density within the limits that we tested. Similar to the results presented in Ref. [14], we observed that with increasing electron dosage, the valence band emission intensity decreases monotonically while a smaller new feature 3.3 eV above the valence band edge emerges. For reasons given in Ref. [14] and discussed in more detail below, we assign the electron irradiation induced band-gap state to the O 2p peak of metal oxide formed during electron irradiation. Fig. 5 shows
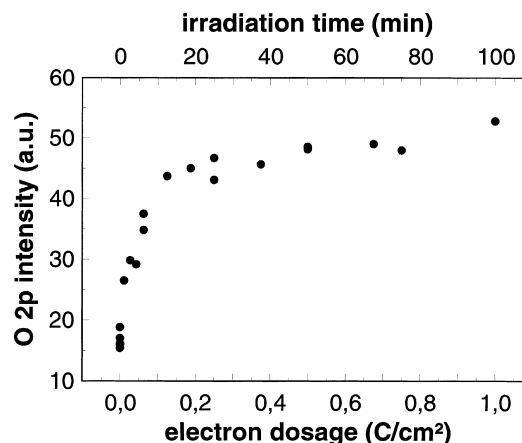
Fig. 5. Development of oxide formation during irradiation of an air-cleaved crystal with 2.5 keV electrons, as measured with ultraviolet photoelectron spectroscopy. The integrated yield of the O 2p peak developing during electron irradiation [14] is plotted as a function of the electron dosage density.

the development of the integrated intensity of the oxide peak as a function of dosage, i.e. irradiation time. It can be seen that up to about 15 min irradiation time corresponding to a dosage of 150 mC/cm², the intensity rises steeply, and then the signal continues rising with a much smaller slope. The curve indicates a slow development towards a saturation level, but this has not been determined in these or any other measurements. A comparison of these results with SFM data obtained under similar irradiation conditions [15], however, allows an interpretation of the curve in the sense of a subdivision into two parts where different processes dominate the oxidation behavior. From the SFM measurements performed under similar experimental conditions, it is known that metal colloids grow during irradiation, but after 15 min, a large fraction of the surface is covered by metal forming an irregular film with an average thickness of about 5 nm. This film effectively shields the surface from incoming electrons, and the production of surface metal is essentially saturated after 20 min. Hence, we anticipate that the slow rise in oxide intensity above the metal saturation dosage density of 150 mC/cm² is due to a reduced interaction of the electrons with the CaF$_2$ crystal. In the region below saturation, however, the oxide production rate may either be determined by the metal production efficiency or the available supply of oxygen.

To clarify this, we performed supplementary measurements with XPS. The sampling depth is smaller in this case, and so we can study oxidation in a surface sheet with a thickness of about 2 nm instead of 6 nm as probed by UPS[1]. Furthermore, in these experiments, we did not measure the amount of oxide present after certain electron doses but monitored oxide formation as a function of time elapsed after irradiation, thus probing thermal diffusion of oxygen to the surface. Samples were irradiated with a dosage density of 100 mC/cm² at 420 K and XPS spectra taken in certain time intervals after irradiation. We specifically observed the temporal development of the O 1s and Ca 2p peaks, respectively. Spectra in the region of these peaks taken prior to electron irradiation and on the fully oxidised surface are displayed in Fig. 6. The O 1s peak is barely measur-
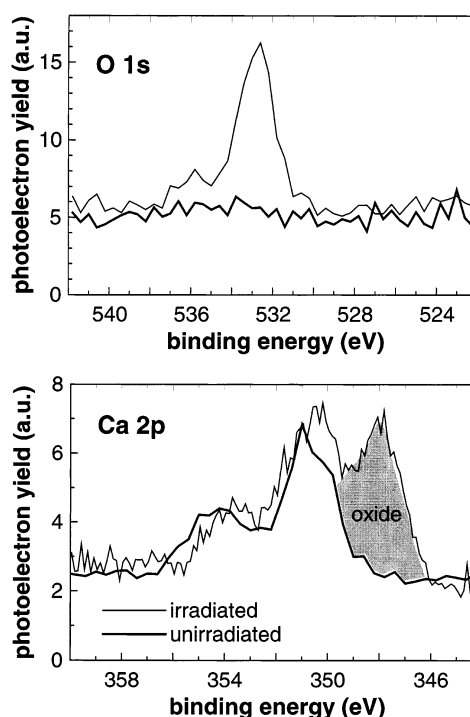


Fig. 6. X-ray photoelectron spectra in the region of the O 1s and Ca 2p peaks for the pristine and electron irradiated CaF$_2$(111) surface. Electron irradiation was performed with 2.5 keV electrons at a dosage density of 100 mC/cm².

able prior to irradiation, whereas it is clearly developed at a binding energy of 532.5 eV after irradiation. In various experiments, the peak position shifted somewhat, but these shifts could clearly be attributed to sample charging by relating the peak position to that of the Ca 2p peak that shifted accordingly. For the discussion in Section 5, it is important to note that we did not observe any significant shift in the O 1s peak that may have indicated the presence of oxygen in a different chemical state from that observed in Fig. 6. In the Ca 2p doublet, however, a significant chemical shift of about 2.5 eV was observed. Most notable was the growth of a new peak at the low-energy side of the doublet during irradiation. The development of this peak reflects the gradual transformation from Ca in its metallic state or bonded in the fluoride to an oxide compound [16].

The temporal development of the ratio of O 1s and Ca 2p integrated intensities after irradiation is

displayed in Fig. 7 for two sets of measurements. In the first set, the sample temperature was kept constant at 400 K, i.e. at the temperature of irradiation. As indicated by the dashed line, data can be described reasonably well by an exponential function, and a rise time of 40 h can be extracted by a fit to the data. In the second set, the temperature was increased to 513 K, and we found a drastically smaller rise time of 1.4 h. This temperature effect has also been observed reproducibly in other measurements not displayed here and will be interpreted in Section 5.

## 5. Discussion and conclusions

The valence band of CaO is mainly formed by the oxygen 2p states [17], and therefore, it is plausible that in UPS, we find a feature similar to that of the fluorine 2p emission from $CaF_2$. However, angle-resolved CaO valence band photoemission spectra for 40.8 eV (He II) photon energy have been calculated, and the predicted spectrum appeared as a one- or two-peak structure strongly depending on the direction of emission [18]. Due to the different structures and lattice constants of Ca and CaO, we expect a polycrystalline growth of oxide rather than a well-ordered layer, and the



Fig. 7. Integrated O 1s X-ray photoemission yield as a function of time after irradiation with 100 mC/cm² of 2.5 keV electrons. The crystal temperature was kept constant at an irradiation temperature of 400 K in the first measurement but fixed at 513 K after irradiation for the second measurement. The dashed and dotted lines are exponential fits yielding time constants for thermally driven surface oxidation.

photoemission spectrum measured in our experiments is expected to be a weighted integral over several directions. This readily explains the flat, structureless peak of the oxide feature observed in our spectra. The measured width of about 4 eV is compatible with the theoretical prediction[3].

Also, our XPS results accord well with the results on oxide formation found in the literature. It is well established that the O 1s peak may be shifted by up to 4 eV when the oxygen is not directly bonded to an alkali but in the form of a hydroxide or molecularly adsorbed water [19]. In adsorption experiments with water on defective $CaF_2$ surfaces, water either adsorbed as a molecule or dissociated to form oxide or hydroxide [20,21]. In the latter case, the O 1s peak is always shifted to a binding energy higher than the value of 532.5 eV observed in our experiments. Since we did not observe any such shifted peaks but did observe the chemically shifted oxide satellite of the Ca 2p peak, we conclude that oxygen is present at our surfaces only in the form of CaO.

Next, we seek explanations for the oxidation curves from Figs. 5 and 7. We exclude oxide formation from the residual gas as the main source for the features observed by estimating the maximum possible amount of oxygen that could be produced by exposure to the residual gas. We assume that a certain metallised surface area is subject to the oxygen partial pressure of the residual gas, and during this exposure, a monolayer of oxide is formed. Further oxidation is much slower, and the monolayer coverage defines the saturation level. The growth of such a monolayer is a function of exposure time, $t$, where the time constant, $\tau$, describes the speed of approach to the saturation coverage:

$$N(t) = N_0(1 - e^{-t/\tau})$$
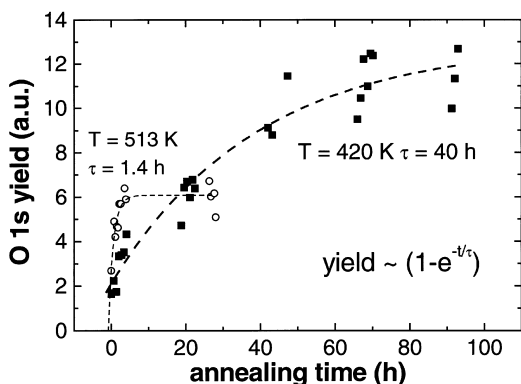
$$\text{with } \tau = \frac{N_0}{\eta P}\sqrt{3mkT}.$$

---

[3] The calculation in Ref. [18] predicts a width of approximately 3 eV. However, for comparable calculations on MgO, it was found that the calculated width of the peak structure is a factor of about 1.4 smaller than the measured width. We assume that a similar correction has to be applied to the comparison for $CaF_2$.

Here, $N(t)$ denotes the number of oxidised surface sites, $N_0$ the number of initially available sites, $\eta$ the sticking coefficient, $P$ the oxygen partial pressure and $T$ the gas temperature ($k$: Boltzmann constant; $m$: oxygen atomic mass). Assuming an upper limit of the oxygen partial pressure of $2 \times 10^{-10}$ Pa and a sticking coefficient of 1, the time constant is about 125 h. This value is much larger than the time constant obtained in the low-temperature oxidation measurement of Fig. 5. XPS measurements at a higher temperature and even more UPS during electron irradiation yield oxidation rates that are several orders of magnitudes larger. Hence, it is clear that there is a source of oxygen in the bulk driving oxidation in the surface layer. It is known from the literature that oxygen may be present in a $CaF_2$ crystal and migrate in the bulk lattice with an activation energy of 0.64 eV [22,23]. Therefore, we conclude that a major part of the observed oxidation is a result of a diffusive process carrying oxygen through the lattice to the metallized surface regions probed by photoelectron spectroscopy. Diffusive oxidation can be described by an exponential function similar to that given for oxidation from the residual gas. In this case, the time constant, $\tau$, is determined by the oxygen diffusivity instead of the gas kinetic parameters and will depend on the sample temperature. This explains well the strong temperature dependence of thermally driven oxidation observed in Fig. 7.

During the action of the electron beam, however, the oxidation cannot be described by a simple exponential function since the number of available oxidation sites, $N_0$, is a function of time in this case. From the dependence of the time constant, $\tau$, on $N_0$, it can be inferred that the production of metal during oxidation, i.e. a rise in $N_0$, will strongly accelerate oxidation. This readily explains the extremely rapid oxidation observed during electron irradiation (Fig. 5) below the saturation dosage for metal production, even at the low irradiation temperature of 420 K. An alternative interpretation is, however, that oxygen transport is driven by electron irradiation. This appears to be plausible if oxygen is present in the crystal in the form of $O^{2-}$ ions, since we have shown recently that fluorine ions are mobilised in the electric field created by low-energy electron irradiation of

$CaF_2$ [13], and the same might apply for oxygen ions. Apparently, oxygen diffusion is already activated at a temperature of 490 K, which compares well with the activation energy of 0.64 eV found in the literature. The fact that oxidation effects are not observed in UHV cleaved crystals [14] shows that in our high-purity crystals, oxygen is not present in a significant quantity at the beginning but is introduced by exposure to ambient air.

Since our spectroscopic experiments are not calibrated, we are not able to determine the concentration of oxygen present in the surface layer after air exposure, and it is not clear a priori whether the oxidation dynamics found in UPS measurements, as shown in Fig. 5, is mainly determined by the metal production rate or the amount of available oxygen. We believe, however, that XPS studies, as shown in Fig. 7 indicate that there is much less oxygen available than metal, and the oxygen concentration is, in fact, the rate-limiting factor. At a dosage density of 100 mC/cm², as applied in the measurements shown in Fig. 7, metallisation has almost reached saturation, and if oxygen were present in large concentrations, most of the metal would be oxidised already during electron irradiation. However, during heating after irradiation, the oxide signal increases by more than 500%, i.e. oxygen present in small concentrations needs time to reach metal clusters to be oxidised by a slow diffusive motion, but this time can be reduced by thermal activation, as demonstrated by the higher temperature measurement.

In summary, we have shown that the exposure of a $CaF_2(111)$ surface to air results in the uptake of a small amount of oxygen by the crystal in a near surface layer and a severe degradation of the surface. The surface structures formed during the degradation are a result of chemical reactions at the surface and were proved to be stable against thermal treatment. The oxygen stored in the crystal can be thermally activated and driven to the surface. When the surface is irradiated with low-energy electrons, diffusion is strongly enhanced, and Ca metal formed by the electron impact is converted into CaO.

Further studies are needed to clarify the role of other components of the air in the surface degradation process. We anticipate that the observed sur-

face patches are compounds containing oxide, hydroxide and carbonate [24] with a very low degree of structural order and that a superposition of occupied electronic states associated with these compounds is the origin of the structureless band-gap emission observed in UPS experiments on air-exposed surfaces. These states, of course, allow a linear interaction of light with a photon energy well below the band-gap energy with the crystal and the band-gap density of states defining the ultimate limit in low linear optical absorption that can presently be obtained for technically relevant surfaces of $CaF_2$ optical components. It might, however, be possible to reverse surface chemical processes by using fluorine [25] and to restore the structurally perfect and stoichiometric surface. In this way, the light damage resistivity of the surface against high-energy pulses could be pushed beyond the present limits.

## Acknowledgements

## References

[1] L. Klocek (Ed.), Handbook of Infrared Materials, Marcel Dekker, New York, 1991, p. 231.
[2] IBM J. Res. Dev. 41 (1–2) (1997).
[3] V. Liberman, M. Rothschild, J.H.C. Sedlacak, R.S. Uttaro, A. Grenville, A.K. Bates, C. Van Peski, Opt. Lett 24 (1) (1999) 58.
[4] M. Reichling, in: J.J. Dubowski, P.E. Dyer (Eds.), Laser Applications in Microelectronic and Optoelectronic Manu-facturing III, SPIE Proc. 3274, Bellingham (1998) 2.
[5] E. Stenzel, S. Gogoll, J. Sils, M. Huisinga, H. Johansen, G. Kästner, M. Reichling, E. Matthias, Appl. Surf. Sci. 109–110 (1997) 162.
[6] H. Johansen, G. Kästner, J. Mater. Sci. 33 (15) (1998) 3839.
[7] R. Bennewitz, M. Reichling, E. Matthias, Surf. Sci. 387 (1–3) (1997) 69.
[8] M. Huisinga, M. Reichling, E. Matthias, Phys. Rev. B 55 (12) (1997) 7600.
[9] N. Itoh, K. Tanimura, Rad. Eff. 98 (1986) 269.
[10] E. Stenzel, N. Bouchaala, S. Gogoll, Th. Klotzbücher, M. Reichling, E. Matthias, in: G.E. Matthews, R.T. Williams (Eds.), Defects in Insulating Materials ICDIM 96 Materi-als Science Forum 239–241, Trans Tech Publications, Zurich, 1997, p. 591.
[11] G. Ertl, J. Küppers, Low Energy Electrons and Surface Chemistry, 2nd edition, VCH Verlagsgesellschaft, Wein-heim, 1985, p. 114.
[12] M. Huisinga, Ph.D. thesis, Freie Universität, Berlin, 1998.
[13] R. Bennewitz, D. Smith, M. Reichling, Phys. Rev. B 59 (12) (1999) 8237.
[14] M. Reichling, M. Huisinga, D. Ochs, V. Kempter, Surf. Sci. 402–404 (1998) 145.
[15] M. Reichling, R.M. Wilson, R. Bennewitz, R.T. Williams, S. Gogoll, E. Stenzel, E. Matthias, Surf. Sci. 366 (1996) 531.
[16] J. Chastain (Ed.), Handbook of X-ray Photoelectron Spectroscopy, Perkin-Elmer Corporation, Eden Prairie, 1992.
[17] V.S. Stepanyuk, A. Szasz, A.A. Grigorenko, A.A. Katsnel-son, O.V. Farberovich, V.V. Mikhalin, A. Hendry, Phys. Stat. Sol. (b) 173 (1992) 633.
[18] M. Grass, J. Braun, G. Borstel, Surf. Sci. 334 (1995) 215.
[19] J.C. Fuggle, L.M. Watson, D.J. Fabian, S. Affrossman, Surf. Sci. 49 (1975) 61.
[20] C. Akita, T. Tomioka, M. Owari, A. Mizuike, Y. Nihei, Jpn. J. Appl. Phys. 29 (10) (1990) 2106.
[21] Y. Wu, J.T. Mayer, E. Garfunkel, T.E. Madey, Langmuir 10 (1994) 1482.
[22] A. Hammou, M. Duclot, V.A. Levitskii, J. de Phys. C7 (Suppl. au No. 12 (tome 37)) (1976) C7–342.
[23] M. Svantner, E. Mariani, Krist. Tech. 13 (12) (1978) 1431.
[24] D. Ochs, B. Braun, W. Maus-Friedrichs, V. Kempter, Surf. Sci. 417 (1998) 406.
[25] I.M. Thomas, Appl. Opt. 27 (16) (1988) 3356.